

Spin and Orbital Magnetism by Light in Rutile Altermagnets

T. Adamantopoulos,^{1,2,*} M. Merte,^{1,2,3} F. Freimuth,³ D. Go,³ M. Ležaić,¹ W. Feng,^{4,5} Y. Yao,^{4,5} J. Sinova,^{3,6} L. Šmejkal,^{3,6} S. Blügel,¹ and Y. Mokrousov^{1,3}

¹*Peter Grünberg Institut, Forschungszentrum Jülich, 52425 Jülich, Germany*

²*Department of Physics, RWTH Aachen University, 52056 Aachen, Germany*

³*Institute of Physics, Johannes Gutenberg University Mainz, 55099 Mainz, Germany*

⁴*Centre for Quantum Physics, Key Laboratory of Advanced Optoelectronic Quantum Architecture and Measurement (MOE), School of Physics, Beijing Institute of Technology, Beijing 100081, China*

⁵*Beijing Key Lab of Nanophotonics and Ultrafine Optoelectronic Systems, School of Physics, Beijing Institute of Technology, Beijing 100081, China*

⁶*Institute of Physics, Czech Academy of Sciences, Cukrovarnická 10, 162 00 Praha 6, Czech Republic*
(Dated: March 18, 2024)

While the understanding of altermagnetism is still at a very early stage, it is expected to play a role in various fields of condensed matter research, for example spintronics, caloritronics and superconductivity. In the field of optical magnetism, it is still unclear to which extent altermagnets as a class can exhibit a distinct behavior. Here we choose RuO₂, a prototype metallic altermagnet with a giant spin splitting, and CoF₂, an experimentally known insulating altermagnet, to study the light-induced magnetism in rutile altermagnets from first-principles. We demonstrate that in the non-relativistic limit the allowed sublattice-resolved orbital response exhibits symmetries, imposed by altermagnetism, which lead to a drastic canting of light-induced moments. On the other hand, we find that inclusion of spin-orbit interaction enhances the overall effect drastically, introduces a significant anisotropy with respect to the light polarization and strongly suppresses the canting of induced moments. Remarkably, we observe that the moments induced by linearly-polarized laser pulses in light altermagnets can even exceed in magnitude those predicted for heavy ferromagnets exposed to circularly polarized light. By resorting to microscopic tools we interpret our results in terms of the altermagnetic spin splittings and of their reciprocal space distribution. Based on our findings, we speculate that optical excitations may provide a unique tool to switch and probe the magnetic state of rutile altermagnets.

Introduction

Recently, altermagnets emerged as a new class of magnetic materials, which combine staggered collinear spin moments in real space, with an alternating spin splitting in the reciprocal space, leading to a perfect compensation of moments as a result of a combined action of time-reversal (\mathcal{T}), or, generally spin rotation symmetries, and crystal symmetries [1, 2]. Due to the inherent spin-splitting of the states of d-, g-, or i-wave form, altermagnets are anticipated to host numerous exotic physical phenomena – a fact that renders them as an extremely attractive platform in the context of spintronics. So far, several works revealed the existence of the anomalous Hall effect in a series of altermagnetic materials, e.g. RuO₂ [3, 4], MnTe [5], SrRuO₃ [6], κ -type organic conductors [7], and perovskites [8], as well as generation of strong spin-polarized currents [9, 10], spin-splitter torque [11–13], spin-pumping [14], and crystal thermal transport [15]. The prospect of altermagnets in the field of optical magnetism has slowly started gaining interest and some initial experimental works studied their behavior upon laser excitation [16–19]. Theoretically, on the other hand, very little is known about the interaction of altermagnets with light.

Among the altermagnetic materials, tetragonal rutile RuO₂ with a $P4_2/mnm$ space group [see Fig. 1(g)] stands as one of the most explored. The theoretically predicted large spin-splitting of 1.3 eV [2, 3, 20] labels RuO₂ as an ideal platform for the observation of emergent altermagnetic phenom-

ena. Despite traditionally being considered a Pauli paramagnet, recently a room-temperature collinear antiparallel magnetic ordering was discovered in both RuO₂ bulk crystals and thin films [21, 22], however, the reported small local magnetization value of $0.05 \mu_B$ still remains an open controversial issue [23]. Among rutile altermagnets another popular representative is CoF₂, which belongs to a family of well-known insulating transition-metal difluorides [24, 25] and which has been extensively studied in the past due to its strong piezomagnetic effect [26–28]. Being isostructural to RuO₂, CoF₂ is an altermagnet with an experimentally measured local magnetization of $2.21 \mu_B$ [29], although the estimated values of the band-gap and of the magnetocrystalline anisotropy energy strongly depend on the first-principles Hubbard parameter U [25]. Due to their structural inversion symmetry, RuO₂ and CoF₂ allow for linear in an electric field currents like anomalous and spin/orbital Hall effects but do not allow for second order photocurrents.

On the other hand, owing to different symmetry requirements, centrosymmetric crystals allow for spin and orbital induced moments, commonly known as the inverse Faraday effect [30, 31], and optical torques on the spins [32], which are second order in applied electric field [33]. The photo-induced magnetism is an important mechanism for optical detection of magnetic order [34], while the optical spin torques have been shown to drive THz emission [35], antiferromagnetic dynamics and switching [36]. In case of antiferromagnets (AFMs), the inverse Faraday effect and optical torques have been studied recently for Mn₂Au [37, 38], however, very little is known about the photo-induced magnetism in altermagnetic materi-

* t.adamantopoulos@fz-juelich.de

als. Here, based on first principles methodology in combination with the Keldysh formalism for photoresponse, we study in detail the light-induced spin and orbital magnetism in rutile RuO_2 and CoF_2 , and discuss the consequences of our findings for the optical control and detection of altermagnetism.

Method

We employ the Keldysh formalism [32, 39] in order to compute the second order induced orbital and spin magnetization with Cartesian component $\delta\mathcal{O}_i$, emerging as a response to a continuous laser pulse of frequency ω according to:

$$\delta\mathcal{O}_i = -\frac{\hbar a_0^3 I}{2c} \frac{\mathcal{E}_H}{(\hbar\omega)^2} \text{Im} \sum_{jk} \epsilon_j \epsilon_k^* \varphi_{ijk}, \quad (1)$$

where $a_0 = 4\pi\epsilon_0\hbar^2/(m_e e^2)$ is the Bohr's radius, $I = \epsilon_0 c E_0^2/2$ is the intensity of the pulse, ϵ_0 is the vacuum permittivity, m_e is the electron mass, e is the elementary charge, \hbar is the reduced Planck constant, c is the light velocity, $\mathcal{E}_H = e^2/(4\pi\epsilon_0 a_0)$ is the Hartree energy, and ϵ_j is the j -th component of the polarization vector of the pulse. The tensor φ_{ijk} (see Eq.(14) of Ref. [32] for a detailed form) is expressed in terms of the Green functions of the system, two velocity operators (v_i and v_j) and the i -th component of the orbital angular momentum (OAM) operator L_i , or the i -th component of the Pauli matrix σ_i . For the orbital response, the prefactor in Eq. (1) must be multiplied by an additional factor of 2. Within the Keldysh formalism, a constant lifetime broadening Γ is introduced to account for effects of disorder on the electronic states.

Symmetry analysis

In order to determine the symmetry allowed components of the tensor φ_{ijk} in Eq. (1) in a compensated AFM, we first need to find out if it transforms like an axial (a), polar (p), staggered axial (sa), or staggered polar (sp) tensor [38]. Then the symmetry allowed components can be found by applying the Neumann's principle.

In the case of the altermagnets considered here we calculate the atom-resolved orbital/spin polarization and then we study separately the overall induced orbital/spin moment in the unit cell, defined as the sum of all induced moments in the unit cell, as well as the staggered component, defined as the difference between the moments on different sublattices: $\delta\mathcal{O}^{\text{stag}} = \frac{1}{2}[\delta\mathcal{O}(\text{Atom}_1) - \delta\mathcal{O}(\text{Atom}_2)]$. At first, we assume that the altermagnets studied here are collinear and fully compensated, which allows to expand the laser-induced response in orders of the Néel vector \mathbf{N} as:

$$\delta\mathcal{O}_i = \varphi_{ijk}^{(3a)} E_j E_k^* + \varphi_{ijkl}^{(4sp)} E_j E_k^* N_l + \varphi_{ijklm}^{(5a)} E_j E_k^* N_l N_m + \dots, \quad (2)$$

for the total responses and

$$\delta\mathcal{O}_i^{\text{stag}} = \varphi_{ijk}^{(3sa)} E_j E_k^* + \varphi_{ijkl}^{(4p)} E_j E_k^* N_l + \varphi_{ijklm}^{(5sa)} E_j E_k^* N_l N_m + \dots, \quad (3)$$

for the staggered responses. Above, $\varphi_{ijk}^{(3a)/(3sa)}$ is a non-staggered/staggered axial tensor of rank 3 that is independent of the staggered magnetization, $\varphi_{ijk}^{(4p)/(4sp)}$ is a

#	$\varphi_{ijk}^{(3a)}$	Remark	#	$\varphi_{ijk}^{(3sa)}$	Remark
1	$\langle xzy \rangle - \langle yzx \rangle$	✓	4	$\langle yzy \rangle - \langle xzx \rangle$	✓
2	$\langle xxy \rangle - \langle zyx \rangle$		5	$\langle yyz \rangle - \langle xxz \rangle$	{4}
3	$\langle xyz \rangle - \langle yxz \rangle$	{1}	6	$\langle zyy \rangle - \langle zxx \rangle$	

TABLE I. Nonstaggered $\varphi_{ijk}^{(3a)}$ and staggered $\varphi_{ijk}^{(3sa)}$ axial tensors of rank 3. ✓: marks the tensors which correctly predict the presented components. A number in {}-brackets specifies the tensor that can be used as a replacement.

#	$\varphi_{ijkl}^{(4sp)}$	Remark	#	$\varphi_{ijkl}^{(4p)}$	Remark
7	$\langle yyyx \rangle + \langle xxxy \rangle$		17	$\langle zzzz \rangle$	✓ ⊥
8	$\langle xxyx \rangle + \langle yyxy \rangle$	✓	18	$\langle xyyx \rangle + \langle yxyx \rangle$	
9	$\langle xyxx \rangle + \langle yxyy \rangle$	{8}	19	$\langle yxyx \rangle + \langle xyxy \rangle$	✓
10	$\langle yxxx \rangle + \langle xyyy \rangle$		20	$\langle xxxx \rangle + \langle yyyy \rangle$	
11	$\langle yzzx \rangle + \langle xzzy \rangle$		21	$\langle xzzx \rangle + \langle yzzy \rangle$	
12	$\langle yzxx \rangle + \langle xzyz \rangle$	⊥	22	$\langle xzxz \rangle + \langle yzyz \rangle$	⊥
13	$\langle zzyx \rangle + \langle zzyx \rangle$	✓	23	$\langle xxzz \rangle + \langle yyzz \rangle$	{22}
14	$\langle zyzx \rangle + \langle zxzy \rangle$	{14}	24	$\langle yyxx \rangle + \langle xxyy \rangle$	{19}
15	$\langle zyxz \rangle + \langle zxyz \rangle$	✓ ⊥	25	$\langle zzzx \rangle + \langle zzyy \rangle$	✓
16	$\langle yxzz \rangle + \langle xyzz \rangle$	{12}	26	$\langle zxxz \rangle + \langle zyzy \rangle$	{25}
			27	$\langle zxxz \rangle + \langle zyyz \rangle$	✓ ⊥

TABLE II. Staggered $\varphi_{ijkl}^{(4sp)}$ and nonstaggered $\varphi_{ijkl}^{(4p)}$ polar tensors of rank 4. ✓: marks the tensors which correctly predict the presented components. ||: The response is nonzero when \mathbf{N} lies in the xy plane. ⊥: The response is nonzero when \mathbf{N} points in the z direction. A number in {}-brackets specifies the tensor that can be used as a replacement.

non-staggered/staggered polar tensor of rank 4 that is odd in the staggered magnetization, and $\varphi_{ijk}^{(5a)/(5sa)}$ is a non-staggered/staggered axial tensor of rank 5 that is even in the staggered magnetization.

For the $P4_2/mnm$ rutile structure of RuO_2 and CoF_2 we find out that 3 nonstaggered and 3 staggered axial tensors of rank 3 are allowed, which are listed in Table I, together with 10 staggered and 11 nonstaggered polar tensors of rank 4, which are listed in Table II. Additionally, our symmetry analysis reveals the existence of 30 nonstaggered and 30 staggered axial tensors of rank 5 that are allowed but not listed here for simplicity, even though we refer to them in the main text. In Tables I and II we use the notation below to refer to the respective tensors of the 4th rank:

$$\delta_{nopq}^{(ijkl)} = \delta_{in} \delta_{jo} \delta_{kp} \delta_{lq} \rightarrow \langle ijkl \rangle, \quad (4)$$

and analogously for the tensors of 3rd and 5th rank. In the following, we compare the results of our ab-initio calculations to the predictions of the symmetry analysis.

Results

Non-relativistic RuO_2

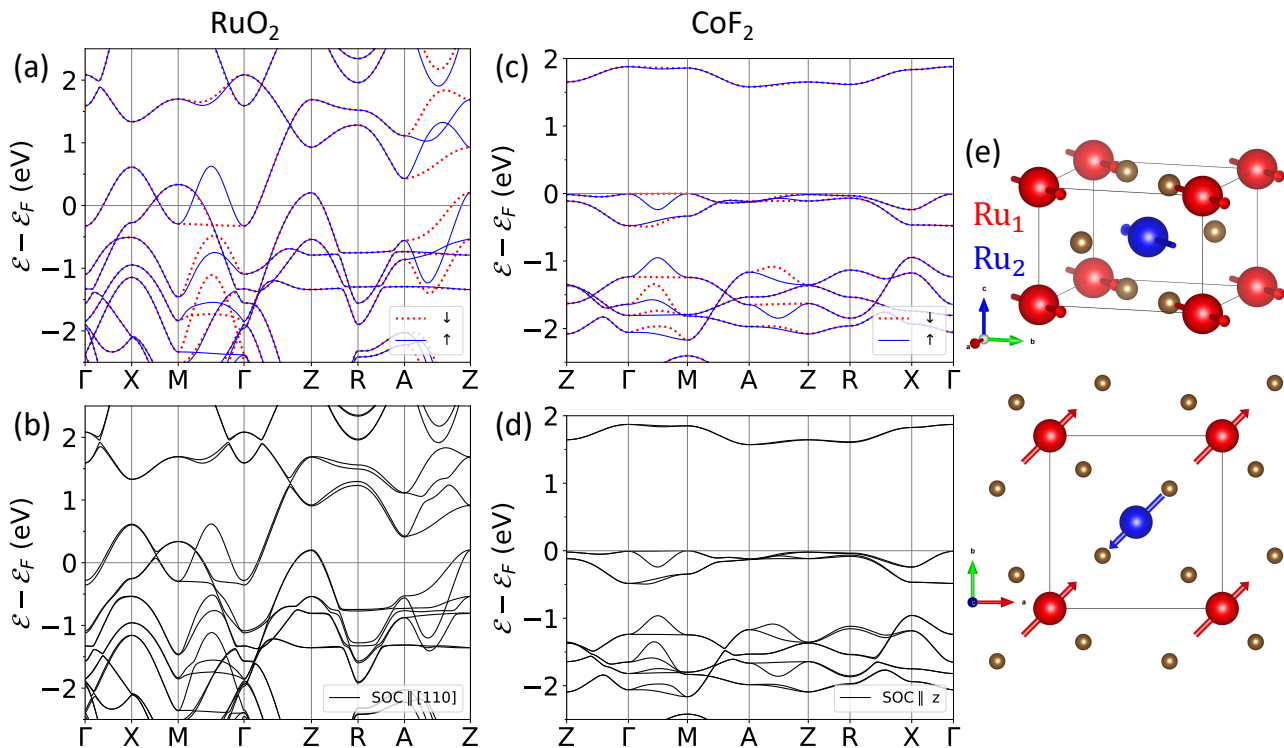


FIG. 1. **Electronic structure of altermagnetic RuO₂ and CoF₂.** (a-b) Bandstructures of non-relativistic (a) and relativistic RuO₂ with \mathbf{N} along [110] (b). (c-d) Bandstructures of non-relativistic (c) and relativistic CoF₂ with \mathbf{N} along the z axis (d). (e) Rutile crystal structure of RuO₂ with staggered magnetization along the [110] direction. The red and blue spheres indicate the Ru atoms in the opposite magnetic sublattices with the respective arrows depicting the magnetic moments. The golden spheres indicate the O atoms. The crystal structure of CoF₂ is identical to that of RuO₂.

First, we explore purely altermagnetic effects, which are not influenced by the presence of spin-orbit coupling (SOC). We begin our discussion by examining the case of non-relativistic RuO₂. The non-relativistic bandstructure of this compound, presented in Fig. 1(a), clearly reflects the large altermagnetic splittings which occur between the spin-up and spin-down states along the M- Γ and A-Z high-symmetry paths. The crystal structure with the magnetic moments pointing along the in-plane [110] direction is shown in Fig. 1(g). As without SOC only orbital photo-response is allowed, in Fig. 2(a) we present the results for the orbital magnetization which is induced by light linearly polarized along the [011] direction in relation to the band filling, decomposed into Ru and spin contributions. At first glance we observe that all corresponding magnetization components are roughly of the same magnitude, leading to an induction of a strongly non-collinear, and not simply staggered response at each Ru atom. The pronounced peaks which appear in the signal can be easily traced back to the altermagnetic splittings of the bands in the energy regions of $[-1.5, -0.5]$ eV and $[+1.0, +2.0]$ eV. Additionally, for the $[-1.5, -0.5]$ eV region there is a contribution originating from flat bands visible along the Γ -Z-R-A-Z path.

The emergence of these specific non-relativistic components can be very well understood from the symmetry analysis for the tensor elements even in \mathbf{N} . This analysis, sum-

marized in Table I and II above, predicts that for light linearly polarized along the [011] direction, δL_x is nonstaggered as reflected in the 3rd rank tensor #1, whereas δL_y is staggered in accord to the 3rd rank tensor #4. The δL_z component is not captured by neither 3rd nor 4th rank tensors, although it is listed in both nonstaggered axial, e.g., $\langle zyxz \rangle - \langle zxyz \rangle$, and staggered axial, e.g., $\langle zyzy \rangle - \langle zxzx \rangle$, 5th rank tensors. Our atom-resolved analysis shows that δL_z is staggered, therefore it is predicted by the 5th rank staggered tensor. We also note that the δL_z response remains unchanged when the crystal is irradiated with light circularly-polarized in the [011] plane (not shown).

The coexistence of staggered and non-staggered components clearly presents a manifestation of the altermagnetic behavior which is expected to incorporate ferromagnetic and antiferromagnetic features. To demonstrate this point more clearly, we perform additional calculations for the orbital non-relativistic photoresponse of the same crystal with oxygen atoms removed. We observe that for this artificial \mathcal{TS} symmetric – where S is spatial inversion \mathcal{P} or translation τ and \mathcal{T} is time reversal – simple tetragonal AFM lattice of Ru atoms the only surviving component is the non-staggered δL_x [shaded black line in Fig. 2(a)], while the staggered components vanish. Additionally, we notice that the components of

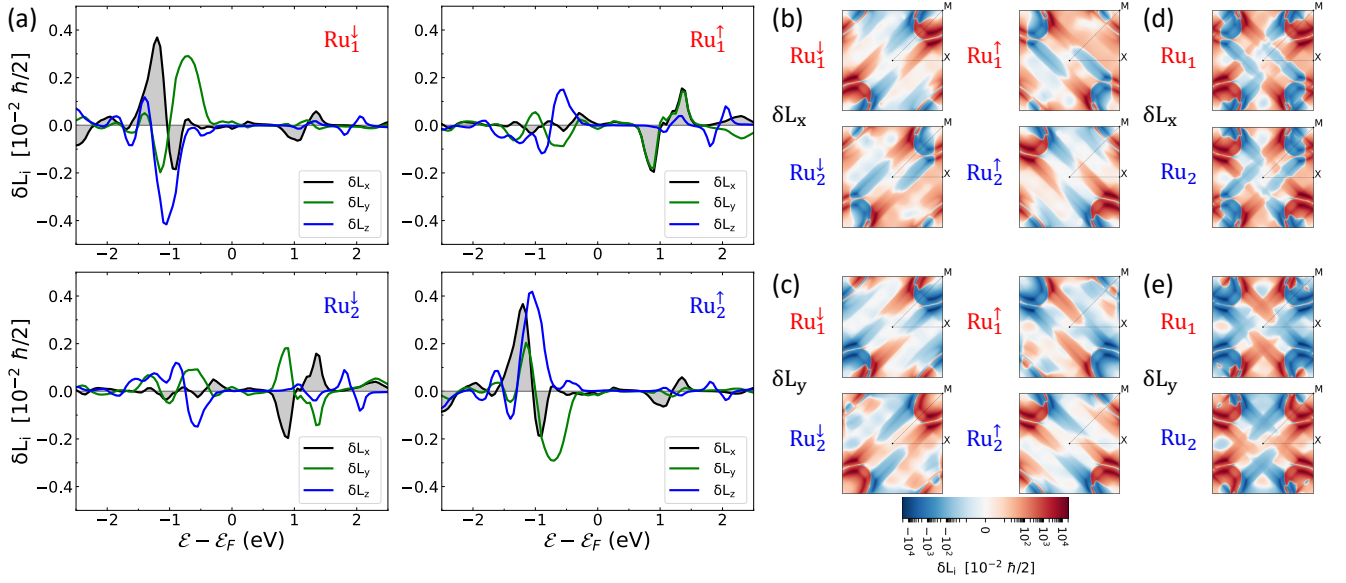


FIG. 2. **Non-collinear spin- and atom-resolved laser-induced orbital magnetization in non-relativistic RuO₂.** (a) Cartesian components of the laser-induced orbital magnetization in relation to the band filling for non-relativistic RuO₂. The spin-resolved (\uparrow vs \downarrow) response is further decomposed into the contributions from two Ru atoms (Ru₁ vs Ru₂). Among the responses, only δL_x (shaded) survives in a system without oxygen atoms, which corresponds to a \mathcal{TS} AFM simple tetragonal lattice of Ru atoms. (b-e): Reciprocal space distribution of laser-induced orbital magnetization in non-relativistic RuO₂. (b-c): Non-staggered δL_x (b) and staggered δL_y (c) components decomposed into Ru contributions for each spin channel. (d-e): Non-staggered δL_x (d) and staggered δL_y (e) components decomposed into Ru contributions and summed over spin directions. The reciprocal space distributions are plotted over the constant energy surface at the true Fermi level \mathcal{E}_F . In all calculations, the light frequency is $\hbar\omega = 0.25$ eV, lifetime broadening $\Gamma = 25$ meV, light is polarized along $[011]$ direction and its intensity is $I = 10$ GW/cm².

$\delta \mathbf{L}$ are connected by the following relations

$$\delta L_x^{\text{Ru}_1^{\uparrow(\downarrow)}} = \delta L_x^{\text{Ru}_2^{\uparrow(\downarrow)}} \quad \text{and} \quad \delta L_{y,z}^{\text{Ru}_1^{\uparrow(\downarrow)}} = -\delta L_{y,z}^{\text{Ru}_2^{\uparrow(\downarrow)}}, \quad (5)$$

for light linearly polarized along $[011]$.

The first relation in Eq. (5) can be proven as follows:

$$\delta L_x^{\text{Ru}_1^{\uparrow}} + \delta L_x^{\text{Ru}_1^{\downarrow}} = \delta L_x^{\text{Ru}_2^{\uparrow}} + \delta L_x^{\text{Ru}_2^{\downarrow}} \quad (6)$$

is a relation that follows from the fact that for light polarization along $[011]$ the response L_x is non-staggered. A second relation follows from the observation that the total response from all the wavefunctions with spin \uparrow has to be equal to the total response from all the wavefunctions with spin \downarrow in this compensated altermagnet computed without SOC:

$$\delta L_x^{\text{Ru}_1^{\uparrow}} + \delta L_x^{\text{Ru}_2^{\uparrow}} = \delta L_x^{\text{Ru}_1^{\downarrow}} + \delta L_x^{\text{Ru}_2^{\downarrow}}. \quad (7)$$

Subtracting Eq. (7) from Eq. (6) and simplifying the result we obtain the first relation in Eq. (5).

In order to obtain the second relation in Eq. (5) we consider the relation

$$\delta L_y^{\text{Ru}_1^{\uparrow}} + \delta L_y^{\text{Ru}_1^{\downarrow}} - \delta L_y^{\text{Ru}_2^{\uparrow}} - \delta L_y^{\text{Ru}_2^{\downarrow}} = 0, \quad (8)$$

which states that the staggered response is zero in this simple crystal structure where the oxygens have been removed. A second relation relevant in this case is

$$\delta L_y^{\text{Ru}_1^{\uparrow}} + \delta L_y^{\text{Ru}_1^{\downarrow}} + \delta L_y^{\text{Ru}_2^{\uparrow}} + \delta L_y^{\text{Ru}_2^{\downarrow}} = 0. \quad (9)$$

This relation states that the total axial response along y is zero for the light polarization here considered. Subtracting these latter two relations from each other we obtain the second part of Eq. (5) for the axial response along y . The axial response along z can be discussed analogously.

The above relations hold true even after summing the contributions of each spin direction on the respective Ru atom (not shown), which is expected from the non-staggered origin of δL_x and the staggered origin of δL_y and δL_z . Similar relations also hold for linear polarization along $[101]$ (not shown), with δL_y assuming the role of the non-staggered component, while the staggered components are δL_x and δL_z , following the symmetry of tensors #1 and #4. Additionally, both our symmetry analysis and our calculations reveal further relations which connect the non-vanishing components for different directions of the linear light polarization vectors:

$$\delta L_x^{\text{Ru}_1^{\uparrow(\downarrow)}/\text{Ru}_2^{\uparrow(\downarrow)}}, \epsilon \parallel [011] = -\delta L_y^{\text{Ru}_1^{\uparrow(\downarrow)}/\text{Ru}_2^{\uparrow(\downarrow)}}, \epsilon \parallel [101] \quad (10)$$

$$\delta L_y^{\text{Ru}_1^{\uparrow(\downarrow)}/\text{Ru}_2^{\uparrow(\downarrow)}}, \epsilon \parallel [011] = -\delta L_x^{\text{Ru}_1^{\uparrow(\downarrow)}/\text{Ru}_2^{\uparrow(\downarrow)}}, \epsilon \parallel [101] \quad (11)$$

$$\delta L_z^{\text{Ru}_1^{\uparrow(\downarrow)}/\text{Ru}_2^{\uparrow(\downarrow)}}, \epsilon \parallel [011] = -\delta L_z^{\text{Ru}_1^{\uparrow(\downarrow)}/\text{Ru}_2^{\uparrow(\downarrow)}}, \epsilon \parallel [101]. \quad (12)$$

Overall, we predict that in the non-relativistic case the optically induced orbital magnetization in rutile altermagnets will have a strongly canted character on neighboring magnetic ions, with the direction and sense of the relative canting controllable by the light polarization. We emphasize that this is a

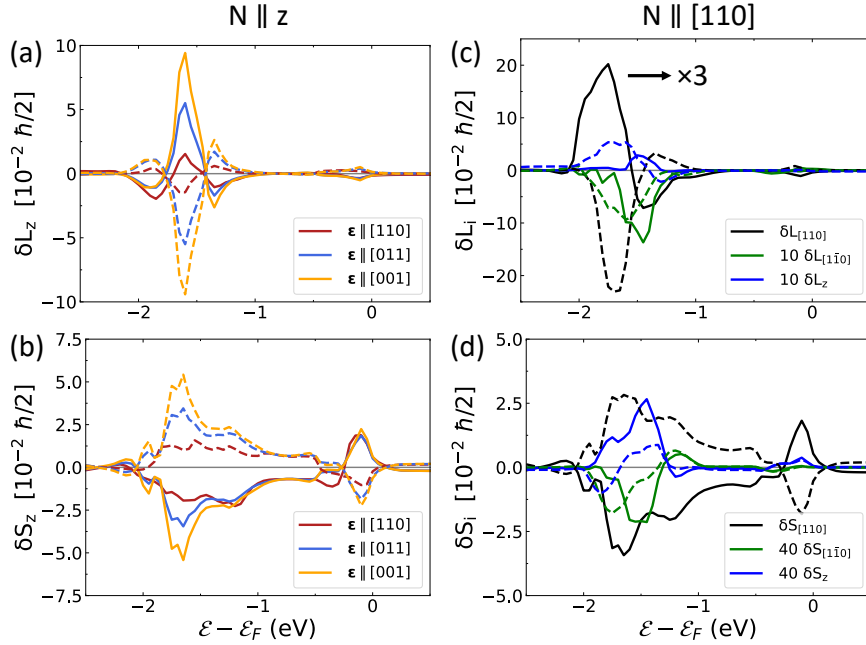


FIG. 3. **Atom-projected laser-induced orbital and spin magnetization in relativistic CoF₂.** (a-b): Orbital (a) and spin (b) z -components of the laser-induced magnetization as a function of the band filling, arising for different cases of linearly polarized light, in CoF₂ with \mathbf{N} along the z axis. In (a-b) the x and y magnetization components are not sizeable and are not shown. (c-d) Orbital (c) and spin (d) laser-induced magnetization in relation to the band filling, arising for linearly polarized light along the [011] direction, in the case of CoF₂ with \mathbf{N} along the [110] direction. Note that in (c-d) the components which are perpendicular to \mathbf{N} are significantly enlarged for comparison. In (a-d) the responses are depicted with either a solid or dashed line for Co₁ and Co₂ atoms, respectively. In all calculations, a light energy of $\hbar\omega = 0.25$ eV, a lifetime broadening $\Gamma = 25$ meV and a light intensity of $I = 10$ GW/cm² were used.

purely altermagnetic effect, as it is absent in \mathcal{TS} AFMs.

To understand better the peculiar symmetry of the orbital response, next, we examine its behavior in the reciprocal space. In Fig. 2(b-c) we present the Ru- and spin-resolved distribution of the induced components δL_x and δL_y in Fig. 2(b) and Fig. 2(c), respectively, as well as their sum over spin in Fig. 2(d) and Fig. 2(e). The distributions are plotted at the true Fermi level for $k_z = 0$, and roughly consist of equal contributions with opposite sign – a behavior which explains their suppression at this energy when integrated over k -space, see Fig 2(a). First of all, all distributions obey an inversion symmetry with respect to Γ and a C_{2z} symmetry with respect to a π -rotation around z . Moreover, we notice that if we apply a $[C_{4z}||M_{[110]}]$ or $[C_{4z}||M_{[1\bar{1}0]}]$ symmetry operation, where C_{4z} is a 4-fold rotation around the z -axis and $M_{[110]}$ ($M_{[1\bar{1}0]}$) is a mirror symmetry with respect to a plane perpendicular to the [110] ([1 $\bar{1}$ 0]) diagonal, the δL_x distribution of the Ru₁[↑] atom becomes equal to the distribution of the Ru₂[↓] atom, with the same also applying for the Ru₁[↓] and Ru₂[↑] atoms. For the δL_y distributions, apart from the aforementioned symmetry operations, a change of sign is also needed to relate the respective atoms. This means that the relations of Eq. (5) hold true in the reciprocal space. We note that the C_{4z} rotation is responsible for interchanging the Ru atoms between the two opposite spin sublattices in RuO₂. Additionally, after summation over the spins in Figs. 2(d-e), the aforementioned sym-

metry operations connect the response on the two Ru atoms, in the same way as Eq. (5) holds true after spin summation.

CoF₂

We continue our discussion by considering the case of altermagnetic rutile CoF₂. In Fig. 1(c) we present a non-relativistic bandstructure and in Fig. 1(d) the bandstructure computed with SOC for the experimentally observed configuration with $\mathbf{N}||z$. We observe a very small difference between the relativistic and the non-relativistic bands on the quantitative level of band dispersions. However, we point out that the band representations induced by the relativistic magnetic and non-relativistic spin symmetries [1] are in general different. For instance, the the band representation at R is double (single) dimensional for the nonrelativistic (relativistic) case. The calculated electronic structure with a bandgap of ~ 2.0 eV and magnetic moments of $2.66\mu_B$ is in accordance with previous first-principles calculations [25]. The altermagnetic splittings, which are again located along the Γ -M and A-Z high-symmetry paths, are much smaller in magnitude in the case of CoF₂ as compared to RuO₂. First we calculate the laser-induced orbital and spin magnetization for the case of relativistic CoF₂ with $\mathbf{N}||z$, presenting the results in Fig. 3(a) and Fig. 3(b), respectively, in relation to the band-filling. The responses are projected onto each Co atom and are drawn with either a solid or dashed line for each one of them. We consider different cases of light polarization and discuss only the

z -component as the x, y -components are more than one order of magnitude smaller.

We observe that both orbital and spin responses become large predominantly in the energy region of $[-2.0, -1.0]$ eV, with the orbital signal being generally almost two times larger and much sharper in energy. This is rather expected given that in this energy region a large number of Co d -states is located giving rise to altermagnetic splittings and flat bands. The highest peak occurs at ~ -1.6 eV reaching values as high as $10^{-1}\hbar/2$ for the induced orbital and $5.0 \cdot 10^{-2}\hbar/2$ for the induced spin moments. We remark that these values may increase even further upon reduction in the broadening value in ultra-clean systems [37, 40, 41]. A closer view at the energy region of $[-2.0, -1.0]$ eV reveals that the sharp peaks in the responses occur because the used laser frequency of $\hbar\omega = 0.25$ eV is similar to the size of the altermagnetic splittings of CoF₂. The fact that the orbital response peaks in this energy range underlines the crystal-field origin of the altermagnetic spin splitting. Correspondingly, a shift in the light frequency to higher values results in a suppression of the orbital signal. We also notice the existence of a smaller peak at ~ -0.2 eV which is larger for the spin response and can be attributed to the small splitting appearing around this energy.

The case of $\mathbf{N}\parallel z$ is highly symmetric with perfectly compensated staggered magnetization, which is also known not to support the anomalous Hall effect [3]. In this case, our symmetry analysis is in perfect accord to the ab-initio calculations. The presented component in response to linear polarization along the [001] direction [yellow line in Fig. 3(a-b)] is staggered, odd in the magnetization, as predicted by the 4th rank tensor #17. The component which arises for light linearly polarized along the [110] direction [red line in Fig. 3(a-b)] appears both as nonstaggered and staggered. The nonstaggered part is odd in the magnetization and predicted by the 4th rank tensor #15. We note that for circular polarization in the [110] plane (not shown), the nonstaggered part is even in the magnetization and predicted by the 3rd rank tensor #2. On the contrary, the staggered part is odd in the magnetization and predicted by the 4th rank tensor #27. Furthermore, when light is linearly polarized along the [011] direction [blue line in Fig. 3(a-b)], a staggered component arises which is odd in the magnetization and occurs as a linear combination of the 4th rank tensors #17 and #27.

Symmetry-wise, the case of CoF₂ with $\mathbf{N}\parallel[110]$ presents a more complex behavior, Fig. 3(c-d), as it allows for ferromagnetic magnetization, as discussed below. When we compare the orbital and spin induced moments in Fig. 3(c-d) to those arising in response to linearly polarized light along the [011] direction for $\mathbf{N}\parallel z$, we observe that among all Cartesian components the orbital signal is two times larger and the spin signal is somewhat smaller, with peaks appearing in the same energy regions. Moreover, we find that the two components perpendicular to \mathbf{N} are small but not vanishing, and we plot them after multiplying with a large factor to enable comparison of the qualitative behavior of all components. Our symmetry analysis, where we expand the tensors only in orders of \mathbf{N} , predicts the components parallel and perpendicular to \mathbf{N} [black and green lines in Fig. 3(c-d), respectively] to be

non-staggered and staggered at the same time, while being even in the magnetization and described by 5th rank tensors, e.g., nonstaggered axial $\langle yzxy \rangle - \langle xxzy \rangle$ and staggered axial, $\langle yzxy \rangle - \langle xzyx \rangle$. Our calculations confirm the simultaneous non-staggered and staggered nature of these components but reveal them to be odd in the magnetization, in contrast to the symmetry expectations. On the other hand, we find the out-of-plane component [blue line in Fig. 3(c-d)] to be non-staggered and staggered at the same time, odd in the magnetization, and described by the 4th rank tensors #13 and #25, in full agreement with our symmetry analysis.

Relativistic RuO₂

We further explore the properties of spin and orbital photoresponse for $\mathbf{N}\parallel[110]$ by coming back to RuO₂, where this situation is much closer to experimentally observed conditions [21, 22]. The main energy scales of the bandstructure for this case, in analogy to CoF₂, do not show remarkable deviations from the non-relativistic bands, Fig. 1(b). The impact of SOC on the photoresponse in RuO₂ is, however, remarkable. In Fig. 4(a-b) we present Ru-resolved orbital and spin moments, which exhibit a very large component parallel to \mathbf{N} for linear polarization along the [110] and [101] directions. After including SOC into account, the responses reach values which are two orders of magnitude larger than in the non-relativistic case, Fig. 2(a), accounting to about $-1.75 \cdot 10^{-1}\hbar/2$ for the orbital and $-8.0 \cdot 10^{-2}\hbar/2$ for the spin channels, developing strong peaks around ~ -1.0 eV and ~ 1.2 eV, which originate in altermagnetic spin splitting. These values stand as colossal, when compared to those due to inverse Faraday effect in much heavier ferromagnets, such as FePt [31, 42], where they reach similar magnitude. The overall range of values induced by SOC is comparable for CoF₂ and RuO₂, which underlines the fact that in contrast to ferromagnets, it is not the strength of the spin-orbit interaction which drives the prominent response.

The orbital response is very different for each Ru atom and also varies for each polarization case. On the other hand, the spin response varies slightly among ruthenia and remains rather insensitive to the change in light polarization. The case with light polarization along [110] [black line in Fig. 4(a-b)] is correctly predicted by our symmetry analysis with the response being non-staggered and staggered at the same time, as described by the 4th rank tensors #8 and #19, and odd in the staggered magnetization. On the contrary, the case with light polarization along the [101] direction [green line in Fig. 4(a-b)] disagrees with our symmetry predictions because even though it is non-staggered and staggered at the same time, as expected, it is odd in the staggered magnetization and not even. This behavior with respect to the staggered magnetization violates the prediction of the 5th rank tensors, e.g., nonstaggered axial $\langle yzxy \rangle - \langle xxzy \rangle$ and staggered axial, $\langle yzxy \rangle - \langle xzyx \rangle$ components.

In order to get further insight into the microscopic behavior of the photo-induced moments, we analyze their anatomy in the reciprocal space. In Fig. 4(c-d) we present the Brillouin zone distribution of the orbital and spin moments, respectively, separately for each Ru atom, and for two different cases of linear polarization. We focus on the component which is parallel to \mathbf{N} and calculate the distributions

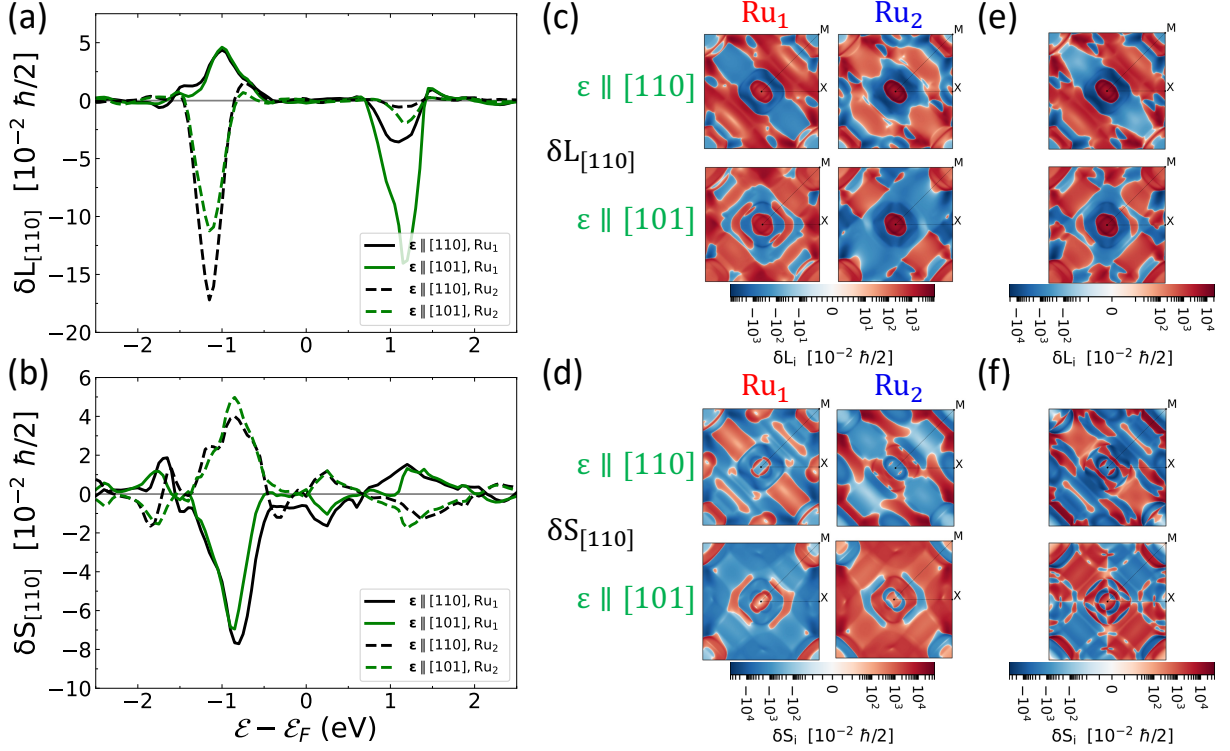


FIG. 4. **Spin and orbital photoresponse in relativistic RuO₂ with N || [110].** (a-b): Orbital (a) and spin (b) laser-induced magnetization in relation to the band filling, arising for linearly polarized light along the [110] or the [101] directions, in the case of RuO₂ with SOC and N along [110]. (c-f): Reciprocal space distribution of laser-induced orbital and spin magnetization, at the shifted Fermi energy level $\mathcal{E}'_F = \mathcal{E}_F - 1.0$ eV. (c-d): Orbital (c) and spin (d) Ru-atom-resolved moments. (e-f): Orbital (e) and spin (f) moments summed on all atoms. In (a-f) only the component parallel to N is sizeable and presented. In (a-b) the responses on the respective Ru atom are depicted with either a solid or dashed line. In (c-d) the left (right) plots present the responses projected on the Ru₁ (Ru₂) atom. In (c-f) the upper (lower) plots present the responses arising for linearly polarized light along the [110] ([101]) direction. In all calculations, a light energy of $\hbar\omega = 0.25$ eV, a lifetime broadening $\Gamma = 25$ meV and a light intensity of $I = 10$ GW/cm² were used.

for the shifted Fermi energy level $\mathcal{E}'_F = \mathcal{E}_F - 1.0$ eV around which the responses in Fig. 4(a-b) peak. The induced moments in Fig. 4(c-d), similarly to the non-relativistic scenario in Fig. 2(d-e), generally consist of large uniform regions of either positive or negative contributions. Qualitatively, we observe that the spin moments in Fig. 4(d) exhibit a sign reversal, when compared to the orbital moments in Fig. 4(c), which is consistent with the integrated responses in Fig. 4(a-b). Moreover, a change of sign also takes place when comparing the distributions between the two Ru atoms [left (right) plots for Ru₁ (Ru₂) in Fig. 4(c-d)], which is especially visible for spin, but much less obvious for the case of the orbital response. This results in very different magnitude of the orbital peaks in the opposite sublattices.

Locally, the spin response exhibits hot spots where its magnitude is larger than the orbital response by an order of magnitude, however, this does not result in a larger overall spin response when integrated over the Brillouin zone. In fact, when the photoresponses are summed over all atoms in the unit cell in Fig. 4(e-f), the orbital distribution in Fig. 4(e) remains rather uniform compared to the spin counterpart in Fig. 4(f), which exhibits a finer structure due to the spin-

splittings brought by SOC having a much weaker effect on the local distribution of orbital moments. In all cases we notice a strong dependence on the light polarization, with drastically different distributions appearing for linear polarization along [110] [upper plots in Fig. 4(c-f)] or [101] [lower plots in Fig. 4(c-f)]. In this relativistic scenario, each distribution in Fig. 4(c-f) still exhibits a C_{2z} rotation and inversion with respect to Γ symmetries in the reciprocal space, but, as opposed to the non-relativistic case, the $[C_{4z} || M_{[110]}]$ symmetry is not even closely preserved.

Further information concerning the microscopic behavior of the studied effects can be derived from the analysis of band-resolved contributions. In Fig. 5(a-b) we present a detailed view of the non-relativistic bands of RuO₂, in the vicinity of the $\mathcal{E}_F - 1.0$ eV energy level, where large alternating splittings appear. For a given (up or down) spin state, we notice a pronounced asymmetry of the bands when moving from M- Γ to Γ -M'. An analysis of the orbital character of the states reveals that L_x [Fig. 5(a)] and L_y [Fig. 5(b)] are equal along the Γ -M' path and opposite along the M- Γ path. Then, in the relativistic scenario, where the states become SOI-entangled, the orbital character in Fig. 5(c) is uniform and preserves the sign

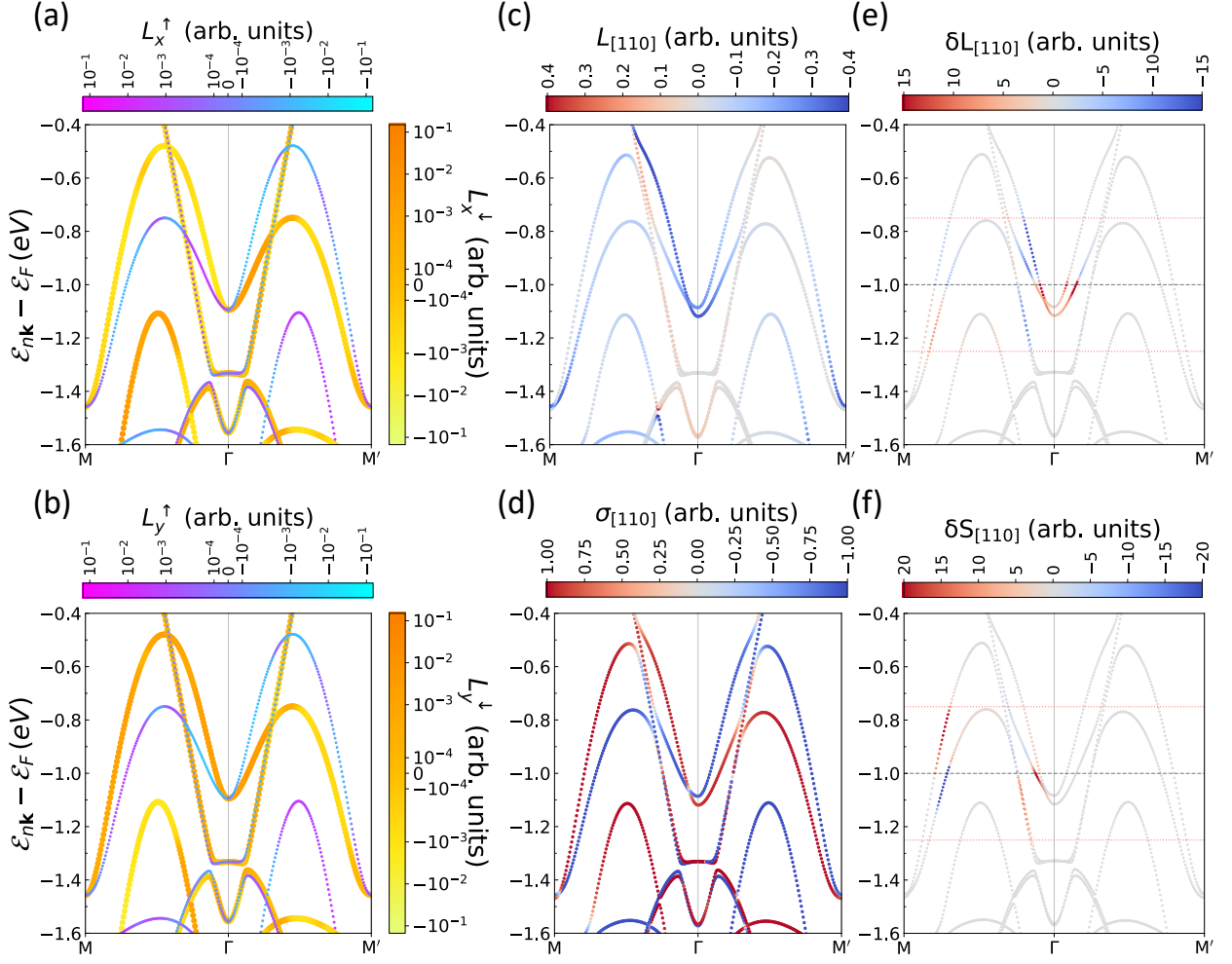


FIG. 5. **Band resolved laser-induced orbital and spin magnetization in RuO₂.** (a-b): Altermagnetic spin-splittings along M–Γ–M′ in the spin-resolved band-structure of non-relativistic RuO₂, colored by the value of (a) L_x and (b) L_y components of the OAM operator. (c-d): Corresponding band-structure of relativistic RuO₂ with $\mathbf{N} \parallel [110]$ colored by the value of the (c) OAM and (d) spin projected onto [110]. (e-f): Band-resolved two-band contributions to the orbital (e) and spin (f) laser-induced moments, at the shifted Fermi energy level $\mathcal{E}'_F = \mathcal{E}_F - 1.0$ eV. The presented components parallel to \mathbf{N} arise for light linearly polarized along the [110] direction. The horizontal dotted red lines at $\mathcal{E}'_F \pm 0.25$ eV denote the laser pulse energy. In (a-f): $\Gamma(0, 0, 0)$, $M(0.5, 0.5, 0)$ and $M'(0.5, -0.5, 0)$.

around Γ point, while the spin character in Fig. 5(d) alternates sign.

Finally, in Fig. 5(e-f) we examine the contribution from the resonant two-band transitions [43] to the band-resolved induced orbital and spin magnetization, respectively, and witness a drastically opposite behavior. While for the orbital response the transitions are mainly located at the center of the Brillouin zone, for the spin response they move further away to the edges. Additionally, the orbital transitions preserve their sign while moving from M– Γ to Γ –M′, whereas the spin transitions are suppressed in the Γ –M′ path. As a result, in case of orbital response, we observe in Fig. 4(e) a uniform feature centered around Γ which strongly contributes to the overall orbital signal. On the other hand, spin response in the vicinity of Γ is driven by isolated hot-spot contributions originating in crossings among bands of opposite spin

hybridizing via SOI. This results in a more “staggered” spin response in the center of the Brillouin zone, Fig. 4(f), in analogy to the case of spin photocurrents in non-centrosymmetric systems [44], which results in an overall suppression of light-induced spin moments.

Beyond altermagnetism

Finally, we come back to the observed inconsistencies between our ab-initio calculations and the predictions of our symmetry analysis. When \mathbf{N} is along z , RuO₂ and CoF₂ are perfectly compensated antiferromagnets. However, as soon as \mathbf{N} is tilted away from z an additional ferromagnetic component $\delta\mathbf{M}$ is induced. $\delta\mathbf{M}$ and \mathbf{N} are related by a staggered polar 2-nd rank tensor, i.e., $\delta M_i = \chi_{ij}^{(2p)} N_j$. In RuO₂ and CoF₂ $\chi_{ij}^{(2p)}$ is required by symmetry to have the form

$$\chi_{ij}^{(2p)} \rightarrow \langle xy \rangle + \langle yx \rangle. \quad (13)$$

Atom	Spin moment	Orbital moment
Ru ₁	1.11979	-0.00245
Ru ₂	-1.12354	-0.01864
O _{1(,2)}	-0.00420	-0.00571
O _{3(,4)}	0.00359	-0.00126

TABLE III. Atom-resolved spin and orbital moments in RuO₂ along \mathbf{N} for $\mathbf{N} \parallel [110]$ (the moments are given in units of μ_B).

Consequently, when \mathbf{N} is along $[110]$, $\delta\mathbf{M}$ is along $[110]$, too. We suggest to refer to this case as *ferri-altermagnetism*. However, when \mathbf{N} is along $[100]$, $\delta\mathbf{M}$ is along $[010]$ implying a small canting. We suggest to denote this case as *canted altermagnetism*.

The size of $\delta\mathbf{M}$ can be estimated most easily from calculations when \mathbf{N} is along $[110]$, because in this case the $\delta\mathbf{M}$ along $[110]$ implies that there is an additional ferromagnetic component parallel to the spin quantization axis – which can be easily extracted from the site-resolved orbital and spin magnetic moments. In Table III we list these site-resolved spin and orbital magnetic moments. We observe that while the spin moments on ruthenia differ by less than $0.004 \mu_B$, an order of magnitude larger difference comes from the orbital channel. Manifestly, the orbital moments on all atoms are aligned, which also explains the consistent sign around Γ in Fig. 5(c). In this context, to underline the orbital origin of the ferromagnetic magnetization, one can refer to this case as *orbital ferri-altermagnet*.

Noteworthy, Eq. (13) does not only apply to the ground-state magnetization, but also to the laser-induced magnetizations. For example $\chi_{ij}^{(2p)}$ implies that the tensor #1, i.e., $\langle xzy \rangle - \langle yzx \rangle$, which describes a non-staggered response, entails a staggered response of the form $\langle yzy \rangle - \langle xzx \rangle$, which is tensor #4. Similar examples are the following pairs of tensors: #12 and #22; #7 and #18; #8 and #19; #10 and #20; #11 and #21; #12 and #22.

Note that $\chi_{ij}^{(2p)}$ predicts the ferri-altermagnetism and the canted altermagnetism only in the relativistic case. In the non-relativistic calculation there are additional symmetries in the spin channel which remove the ferri-altermagnetism and the canting leading to a perfectly compensated altermagnet. However, even in the non-relativistic case $\chi_{ij}^{(2p)}$ predicts the laser-induced staggered orbital response to be related to the non-staggered one in terms of symmetry. Therefore, $\chi_{ij}^{(2p)}$ predicts the coexistence of staggered and non-staggered orbital responses even in the non-relativistic case – in harmony with the discussion in the section “Non-relativistic RuO₂”.

The question arises of whether Eq. (13) is sufficient to explain all aspects of the magnetic structure when \mathbf{N} is tilted away from the z axis. Clearly, there may be additional higher-order corrections. Consider, for example, the 3rd rank axial tensor #2, which is given by $\langle zxy \rangle - \langle zyx \rangle$. Obviously, it al-

lows the coupling

$$\delta N_z = \phi_{zxy}^{(3a)} N_x \delta M_y, \quad (14)$$

i.e., an additional staggered component along z is added to the magnetization, when \mathbf{N} is mainly along x , but when a small ferromagnetic component is added along y due to Eq. (13) as discussed above.

In the following we give an example of how this coexistence of various staggered magnetizations and cantings affects the symmetry analysis. Since the 5-th rank axial tensor

$$\phi_{ijklm}^{(5a)} \rightarrow \langle yzxyy \rangle - \langle xzyxx \rangle \quad (15)$$

is allowed by symmetry,

$$\delta \mathcal{O}_y^{(a,\text{odd})} = \phi_{yzxyy}^{(5a)} \delta N_z N_x \delta M_y \delta \mathcal{O}_y^{(a,\text{even})} \quad (16)$$

predicts a non-staggered axial response along y , which is odd in the magnetization, when $\mathcal{O}_y^{(a,\text{even})}$ is a non-staggered axial response along y even in the magnetization. For example, tensor #1 predicts a response of the type $\mathcal{O}_y^{(a,\text{even})}$, when the polarization vector of the laser pulse is along $[101]$. Adding these two contributions, $\delta \mathcal{O}_y^{(a,\text{odd})}$ and $\delta \mathcal{O}_y^{(a,\text{even})}$, we obtain a result that is neither odd nor even in \mathbf{N} . In fact, the major discrepancy between our *ab-initio* calculations and our simplified symmetry analysis based on an expansion in \mathbf{N} only is the observation that the *ab-initio* results are typically neither odd nor even in \mathbf{N} once \mathbf{N} is tilted away from z , while the symmetry analysis predicts them to be strictly odd or even. This example explains how this discrepancy may be resolved by considering all aspects of the magnetic structure, which generally cannot be captured by a single \mathbf{N} .

Alternatively, one may – of course – obtain the contribution Eq. (16) also directly from the 6th rank polar tensor

$$\phi_{ijklmn}^{(6p)} \rightarrow \langle yzxyzx \rangle + \langle xzyxzy \rangle \quad (17)$$

according to the equation

$$\delta \mathcal{O}_y^{(a,\text{odd})} = \phi_{yzxyzx}^{(6p)} \delta N_z N_x \delta M_y E_z E_x^* \quad (18)$$

in the case where the laser-field polarization is along $[101]$.

The examples above are sufficient to convey the ideas necessary to extend the simplified symmetry analysis in the general case of \mathbf{N} tilted away from z , while a comprehensive symmetry analysis for this general situation is very cumbersome and is beyond the scope of this work.

Discussion

One of the key results of our paper are Eqs. (5)–(12) which establish a “geometric” canted non-relativistic response of the orbital magnetization to incoming linearly-polarized light in rutile altermagnets, where the staggered and non-staggered nature of the components is determined by the orientation of the light polarization with respect to the crystal structure. This canting effect arises as a direct consequence of altermagnetic symmetries, and does not exist in \mathcal{TS} -symmetric AFMs. The conclusions of our work are thus generic for all representatives of the rutile altermagnetic class. The degree of canting

between the induced moments depends on the relative magnitude of the Cartesian components – which are in principle uncorrelated material-specific quantities – and may even vanish in case one of the components accidentally turns to zero. As the effect is even in \mathbf{N} , it is of purely crystal origin, and may be used to determine the crystal structure of rutile altermagnets given that a direct access to the photo-induced moments for different sense of linearly-polarized light is possible, and – importantly – that it can be disentangled from the SOC-induced contributions.

While serving as prototype altermagnets, rutile materials studied in this work are centrosymmetric. This implies, that in contrast to such \mathcal{TS} -symmetric AFMs as Mn_2Au [45] or CuMnAs [46], rutile altermagnets do not allow for Néel type of torques and spin-orbit torque switching in linear response. In this situation, optical torques, which from the viewpoint of symmetry can be directly associated with optically induced second-order transverse spin moments [32], present a unique tool for switching the altermagnetic order by light. Such optical torques have been predicted and observed in experiments on ferromagnets [47], they were shown to serve as a distinct source of THz emission [35], and it was demonstrated that they can trigger optical switching of AFM order in \mathcal{TS} -case [36]. Our non-relativistic calculations predict a staggered “built-in” orbital response, which, when directly translated into proportional values of spin in a very naive way, implies a staggered spin component and thus a possibility of optical switching of altermagnetism by optical torques. Since the orbital moments do not interact with exchange field directly, SOI is required to translate orbital magnetism into non-equilibrium spin density and thus to exert optical torques.

Without SOC, as we have seen, the values of non-relativistic orbital moments induced by light are already very large, exceeding in magnitude the orbital moments in the ground state, see Table III. Our results demonstrate a drastic impact of SOC on spin and orbital photoresponse. First of all, this manifests in a dramatic increase of induced local spin and orbital moments along the direction of the Néel vector. The values that can be induced here under considered experimental conditions can result in a net magnetization of about $0.2 \mu_B$, which already lies in the ballpark of the local staggered spin moments in the ground state of RuO_2 [21]. Among ferromagnets subject to circularly polarized light, this order of magnitude is achievable under normal conditions only for materials containing heavy elements [32, 48]. Such large values can significantly impact the optically-driven dynamics of the magnetization e.g. when exposed to an external magnetic field in an all-optical-switching type of experiments [49, 50]. Detecting this magnetization by MOKE-based techniques [51] may provide a robust way to determine the direction of the Néel vector in altermagnets.

Manifestly, depending on the direction of Néel vector, the SOC-mediated spin and orbital response is not equivalent among the two types of atoms. On the background of large longitudinal induced moments, the transverse moments appear very small, which particularly concerns the case of spin. The same effect of dominant longitudinal response has been also predicted recently for the inverse Faraday effect in \mathcal{TS} -

symmetric Mn_2Au [37]. However, in the case of considered here altermagnets the transverse induced spin and orbital moments possess comparable staggered and non-staggered components at the same time, in analogy to the induced moments along the Néel vector. This implies that upon irradiation by light possibly accompanied by a simultaneous application of a magnetic field, depending on polarization of light and direction of the Néel vector, the spins on opposite sublattices will experience radically different optical torques, while the non-equivalent modifications in the length of the spin moments may give rise to dynamical effects typical of ferrimagnets [48]. It remains to be explored what complex dynamical regimes can be achieved by light in rutile altermagnets, and what consequences this will have for the staggered magnetization switching, domain wall motion and terahertz radiation by altermagnetism.

Computational details The first-principles electronic structures of RuO_2 and CoF_2 were calculated by using the full-potential linearized augmented plane wave FLEUR code [52]. Exchange and correlation effects were treated with the non-relativistic PBE [53] functional, whereas for relativistic effects the second-variation scheme [54] was employed. The lattice parameters of RuO_2 were chosen as $a = 4.543 \text{ \AA}$ and $c = 3.140 \text{ \AA}$ [55] and of CoF_2 as $a = 4.6954 \text{ \AA}$ and $c = 3.1774 \text{ \AA}$ [25]. The muffin-tin radii of Ru and O atoms were set to 2.31 \AA and 1.30 \AA , respectively, whereas of Co and F atoms were set to 2.38 \AA and 1.34 \AA , respectively. The plane-wave cutoff K_{max} was set to 4.5 \AA^{-1} and 4.4 \AA^{-1} for RuO_2 and CoF_2 , respectively. The semicore $4s$ and $4p$ states of Ru as well as the $3s$ and $3p$ states of Co were treated as local orbitals [56]. Regarding self-consistent calculations in the Brillouin zone we used a set of 140 k -points for RuO_2 and a set of 90 k -points for CoF_2 . The AFM ground state configurations were obtained by the use of a Hubbard parameter $U = 2.0 \text{ eV}$ for the $4d$ states of Ru and $U = 1.36 \text{ eV}$ for the $3d$ states of Co, and were consistent with previous first-principles reports on RuO_2 [3] and CoF_2 [25].

Next, we constructed maximally-localized Wannier functions (MLWFs) by employing the Wannier90 code [57], where for the initial projections we chose s and d orbitals for Ru and Co atoms, and p orbitals for O and F atoms. We constructed 48 MLWFs out of 72 Bloch functions (BFs) on a $8 \times 8 \times 8$ k -mesh, with a frozen window of 4.0 eV above the Fermi energy for RuO_2 and 6.5 eV above the Fermi energy for CoF_2 . Our post-processing interpolating calculations of the laser-induced orbital and spin magnetizations were performed on a $128 \times 128 \times 128$ k -mesh which was sufficient to obtain well-converged results. In all calculations the lifetime broadening Γ was set at 25 meV , the light energy $\hbar\omega$ at 0.25 meV , the intensity of light at 10 GW/cm^2 , and we covered an energy region of $[-2.5, 2.5] \text{ eV}$ around the Fermi energy level \mathcal{E}_F .

Acknowledgements

This work was supported by the Deutsche Forschungsgemeinschaft (DFG, German Research Foundation) – TRR 173/2 – 268565370, TRR 288 – 422213477, Joint Sino-German Research Projects (Chinese Grant No. 12061131002 and DFG Grant No. 44880005), and the Sino-German Mobility Programme (Grant No. M-0142). W.F. and Y.Y. are

supported by the NSF of China (Grant Nos. 12274027, 12321004 12234003). This project has received funding from the European Union's Horizon 2020 research and innovation programme under the Marie Skłodowska-Curie grant agree-

ment No 861300. We also gratefully acknowledge the Jülich Supercomputing Centre and RWTH Aachen University for providing computational resources under projects jiff40 and jara0062.

-
- [1] L. Šmejkal, J. Sinova, and T. Jungwirth, Beyond Conventional Ferromagnetism and Antiferromagnetism: A Phase with Non-relativistic Spin and Crystal Rotation Symmetry, *Phys. Rev. X* **12**, 031042 (2022).
- [2] L. Šmejkal, J. Sinova, and T. Jungwirth, Emerging Research Landscape of Altermagnetism, *Phys. Rev. X* **12**, 040501 (2022).
- [3] L. Šmejkal, R. González-Hernández, T. Jungwirth, and J. Sinova, Crystal time-reversal symmetry breaking and spontaneous Hall effect in collinear antiferromagnets, *Science Advances* **6**, eaaz8809 (2020), <https://www.science.org/doi/pdf/10.1126/sciadv.aaz8809>.
- [4] Z. Feng, X. Zhou, L. Šmejkal, L. Wu, Z. Zhu, H. Guo, R. González-Hernández, X. Wang, H. Yan, P. Qin, X. Zhang, H. Wu, H. Chen, Z. Meng, L. Liu, Z. Xia, J. Sinova, T. Jungwirth, and Z. Liu, An anomalous Hall effect in altermagnetic ruthenium dioxide, *Nature Electronics* **5**, 735 (2022).
- [5] R. D. Gonzalez Betancourt, J. Zubáč, R. Gonzalez-Hernandez, K. Geishendorf, Z. Šobáň, G. Springholz, K. Olejník, L. Šmejkal, J. Sinova, T. Jungwirth, S. T. B. Goennenwein, A. Thomas, H. Reichlová, J. Železný, and D. Kriegner, Spontaneous Anomalous Hall Effect Arising from an Unconventional Compensated Magnetic Phase in a Semiconductor, *Phys. Rev. Lett.* **130**, 036702 (2023).
- [6] K. Samanta, M. Ležaić, M. Merte, F. Freimuth, S. Blügel, and Y. Mokrousov, Crystal Hall and crystal magneto-optical effect in thin films of SrRuO₃, *Journal of Applied Physics* **127**, 213904 (2020), https://pubs.aip.org/aip/jap/article-pdf/doi/10.1063/5.0005017/15246940/213904.1_online.pdf.
- [7] M. Naka, S. Hayami, H. Kusunose, Y. Yanagi, Y. Motome, and H. Seo, Anomalous Hall effect in κ -type organic antiferromagnets, *Phys. Rev. B* **102**, 075112 (2020).
- [8] M. Naka, Y. Motome, and H. Seo, Anomalous Hall effect in antiferromagnetic perovskites, *Phys. Rev. B* **106**, 195149 (2022).
- [9] M. Naka, S. Hayami, H. Kusunose, Y. Yanagi, Y. Motome, and H. Seo, Spin current generation in organic antiferromagnets, *Nature Communications* **10**, 4305 (2019).
- [10] A. Bose, N. J. Schreiber, R. Jain, D.-F. Shao, H. P. Nair, J. Sun, X. S. Zhang, D. A. Muller, E. Y. Tsybal, D. G. Schlom, and D. C. Ralph, Tilted spin current generated by the collinear antiferromagnet ruthenium dioxide, *Nature Electronics* **5**, 267 (2022).
- [11] R. González-Hernández, L. Šmejkal, K. Výborný, Y. Yahagi, J. Sinova, T. c. v. Jungwirth, and J. Železný, Efficient Electrical Spin Splitter Based on Nonrelativistic Collinear Antiferromagnetism, *Phys. Rev. Lett.* **126**, 127701 (2021).
- [12] H. Bai, L. Han, X. Y. Feng, Y. J. Zhou, R. X. Su, Q. Wang, L. Y. Liao, W. X. Zhu, X. Z. Chen, F. Pan, X. L. Fan, and C. Song, Observation of Spin Splitting Torque in a Collinear Antiferromagnet RuO₂, *Phys. Rev. Lett.* **128**, 197202 (2022).
- [13] S. Karube, T. Tanaka, D. Sugawara, N. Kadoguchi, M. Kohda, and J. Nitta, Observation of Spin-Splitter Torque in Collinear Antiferromagnetic RuO₂, *Phys. Rev. Lett.* **129**, 137201 (2022).
- [14] C. Sun and J. Linder, Spin pumping from a ferromagnetic insulator into an altermagnet, *Phys. Rev. B* **108**, L140408 (2023).
- [15] X. Zhou, W. Feng, R.-W. Zhang, L. Šmejkal, J. Sinova, Y. Mokrousov, and Y. Yao, Crystal Thermal Transport in Altermagnetic RuO₂, *Phys. Rev. Lett.* **132**, 056701 (2024).
- [16] E. A. Mashkovich, K. A. Grishunin, R. M. Dubrovin, A. K. Zvezdin, R. V. Pisarev, and A. V. Kimel, Terahertz light-driven coupling of antiferromagnetic spins to lattice, *Science* **374**, 1608 (2021), <https://www.science.org/doi/pdf/10.1126/science.abk1121>.
- [17] F. Formisano, R. M. Dubrovin, R. V. Pisarev, A. M. Kalashnikova, and A. V. Kimel, Laser-induced THz magnetism of antiferromagnetic CoF₂, *Journal of Physics: Condensed Matter* **34**, 225801 (2022).
- [18] H. Qiu, T. S. Seifert, L. Huang, Y. Zhou, Z. Kašpar, C. Zhang, J. Wu, K. Fan, Q. Zhang, D. Wu, T. Kampfrath, C. Song, B. Jin, J. Chen, and P. Wu, Terahertz Spin Current Dynamics in Antiferromagnetic Hematite, *Advanced Science* **10**, 2300512 (2023), <https://onlinelibrary.wiley.com/doi/pdf/10.1002/advs.202300512>.
- [19] Y. Liu, H. Bai, Y. Song, Z. Ji, S. Lou, Z. Zhang, C. Song, and Q. Jin, Inverse Altermagnetic Spin Splitting Effect-Induced Terahertz Emission in RuO₂, *Advanced Optical Materials* **11**, 2300177 (2023), <https://onlinelibrary.wiley.com/doi/pdf/10.1002/adom.202300177>.
- [20] O. Fedchenko, J. Minár, A. Akashdeep, S. W. D'Souza, D. Vasilyev, O. Tkach, L. Odenbreit, Q. Nguyen, D. Kutnyakhov, N. Wind, L. Wenthaus, M. Scholz, K. Rossnagel, M. Hoesch, M. Aeschlimann, B. Stadtmüller, M. Kläui, G. Schönhense, T. Jungwirth, A. B. Hellenes, G. Jakob, L. Šmejkal, J. Sinova, and H.-J. Elmers, Observation of time-reversal symmetry breaking in the band structure of altermagnetic RuO₂, *Science Advances* **10**, eadj4883 (2024), <https://www.science.org/doi/pdf/10.1126/sciadv.adj4883>.
- [21] T. Berlijn, P. C. Snijders, O. Delaire, H.-D. Zhou, T. A. Maier, H.-B. Cao, S.-X. Chi, M. Matsuda, Y. Wang, M. R. Koehler, P. R. C. Kent, and H. H. Weitering, Itinerant Antiferromagnetism in RuO₂, *Phys. Rev. Lett.* **118**, 077201 (2017).
- [22] Z. H. Zhu, J. Stempffer, R. R. Rao, C. A. Occhialini, J. Pelli-ciari, Y. Choi, T. Kawaguchi, H. You, J. F. Mitchell, Y. Shao-Horn, and R. Comin, Anomalous Antiferromagnetism in Metallic RuO₂ Determined by Resonant X-ray Scattering, *Phys. Rev. Lett.* **122**, 017202 (2019).
- [23] A. Smolyanyuk, I. I. Mazin, L. Garcia-Gassull, and R. Valentí, Fragility of the magnetic order in the prototypical altermagnet RuO₂ (2024), [arXiv:2310.06909 \[cond-mat.mtrl-sci\]](https://arxiv.org/abs/2310.06909).
- [24] J. W. Stout and S. A. Reed, The Crystal Structure of MnF₂, FeF₂, CoF₂, NiF₂ and ZnF₂, *Journal of the American Chemical Society* **76**, 5279 (1954).
- [25] C. A. Corrêa and K. Výborný, Electronic structure and magnetic anisotropies of antiferromagnetic transition-metal difluorides, *Phys. Rev. B* **97**, 235111 (2018).
- [26] A. S. Borovik-Romanov, Piezomagnetism in the antiferromagnetic fluorides of cobalt and manganese, *J. Exp. Theor. Phys.* **38**, 1088 (1960).
- [27] N. F. Kharchenko, A. V. Bibik, and V. V. Eremenko, Quadratic magnetic rotation of the polarization plane of light in the antiferromagnet CoF₂, *Pis'ma v ZhETF* **42**, 447 (1985).

- [28] N. Kharchenko, R. Szymczak, and M. Baran, Quadratic in field contribution to the magnetization of antiferromagnetic CoF_2 , *Journal of Magnetism and Magnetic Materials* **140-144**, 161 (1995), International Conference on Magnetism.
- [29] J. Strempler, U. Rütt, S. P. Bayrakci, T. Brückel, and W. Jauch, Magnetic properties of transition metal fluorides MF_2 ($M = \text{Mn}, \text{Fe}, \text{Co}, \text{Ni}$) via high-energy photon diffraction, *Phys. Rev. B* **69**, 014417 (2004).
- [30] M. Battiato, G. Barbalinardo, and P. M. Oppeneer, Quantum theory of the inverse Faraday effect, *Phys. Rev. B* **89**, 014413 (2014).
- [31] M. Berritta, R. Mondal, K. Carva, and P. M. Oppeneer, Ab Initio Theory of Coherent Laser-Induced Magnetization in Metals, *Phys. Rev. Lett.* **117**, 137203 (2016).
- [32] F. Freimuth, S. Blügel, and Y. Mokrousov, Laser-induced torques in metallic ferromagnets, *Phys. Rev. B* **94**, 144432 (2016).
- [33] C. Xiao, W. Wu, H. Wang, Y.-X. Huang, X. Feng, H. Liu, G.-Y. Guo, Q. Niu, and S. A. Yang, Time-Reversal-Even Nonlinear Current Induced Spin Polarization, *Phys. Rev. Lett.* **130**, 166302 (2023).
- [34] A. Kirilyuk, A. V. Kimel, and T. Rasing, Ultrafast optical manipulation of magnetic order, *Rev. Mod. Phys.* **82**, 2731 (2010).
- [35] T. J. Huisman, R. V. Mikhaylovskiy, J. D. Costa, F. Freimuth, E. Paz, J. Ventura, P. P. Freitas, S. Blügel, Y. Mokrousov, T. Rasing, and A. V. Kimel, Femtosecond control of electric currents in metallic ferromagnetic heterostructures, *Nature Nanotechnology* **11**, 455 (2016).
- [36] J. L. Ross, P.-I. Gavriloaea, F. Freimuth, T. Adamantopoulos, Y. Mokrousov, R. F. L. Evans, R. Chantrell, R. M. Otxoa, and O. Chubykalo-Fesenko, *Antiferromagnetic Switching in Mn_2Au Using a Novel Laser Induced Optical Torque on Ultrafast Timescales* (2023), [arXiv:2311.00155 \[cond-mat.mtrl-sci\]](https://arxiv.org/abs/2311.00155).
- [37] M. Merte, F. Freimuth, D. Go, T. Adamantopoulos, F. R. Lux, L. Plucinski, O. Gomonay, S. Blügel, and Y. Mokrousov, Photocurrents, inverse Faraday effect, and photospin Hall effect in Mn_2Au , *APL Materials* **11**, 071106 (2023), <https://pubs.aip.org/aip/apm/article-pdf/doi/10.1063/5.0149955/18024264/071106.1.5.0149955.pdf>.
- [38] F. Freimuth, S. Blügel, and Y. Mokrousov, Laser-induced torques in metallic antiferromagnets, *Phys. Rev. B* **103**, 174429 (2021).
- [39] F. Freimuth, S. Blügel, and Y. Mokrousov, Charge and spin photocurrents in the Rashba model, *Phys. Rev. B* **103**, 075428 (2021); F. Freimuth, S. Blügel, and Y. Mokrousov, Laser-induced currents of charge and spin in the Rashba model (2017), [arXiv:1710.10480 \[cond-mat.mes-hall\]](https://arxiv.org/abs/1710.10480).
- [40] X. Mu, Y. Pan, and J. Zhou, Pure bulk orbital and spin photocurrent in two-dimensional ferroelectric materials, *npj Computational Materials* **7**, 61 (2021).
- [41] J. Zhou, Photo-magnetization in two-dimensional sliding ferroelectrics, *npj 2D Materials and Applications* **6**, 15 (2022).
- [42] F. Freimuth, S. Blügel, and Y. Mokrousov, Charge and spin photocurrents in the Rashba model, *Phys. Rev. B* **103**, 075428 (2021).
- [43] T. Adamantopoulos, M. Merte, D. Go, F. Freimuth, S. Blügel, and Y. Mokrousov, Laser-induced charge and spin photocurrents at the BiAg_2 surface: A first-principles benchmark, *Phys. Rev. Res.* **4**, 043046 (2022).
- [44] T. Adamantopoulos, M. Merte, D. Go, F. Freimuth, S. Blügel, and Y. Mokrousov, Orbital Rashba Effect as a Platform for Robust Orbital Photocurrents, *Phys. Rev. Lett.* **132**, 076901 (2024).
- [45] S. Reimers, Y. Lytvynenko, Y. R. Niu, E. Golias, B. Sarpi, L. S. I. Veiga, T. Denneulin, A. Kovács, R. E. Dunin-Borkowski, J. Bläßer, M. Kläui, and M. Jourdan, Current-driven writing process in antiferromagnetic Mn_2Au for memory applications, *Nature Communications* **14**, 1861 (2023).
- [46] P. Wadley, B. Howells, J. Železný, C. Andrews, V. Hills, R. P. Campion, V. Novák, K. Olejník, F. Maccheronzi, S. S. Dhesi, S. Y. Martin, T. Wagner, J. Wunderlich, F. Freimuth, Y. Mokrousov, J. Kuneš, J. S. Chauhan, M. J. Grzybowski, A. W. Rushforth, K. W. Edmonds, B. L. Gallagher, and T. Jungwirth, Electrical switching of an antiferromagnet, *Science* **351**, 587 (2016), <https://www.science.org/doi/pdf/10.1126/science.aab1031>.
- [47] G.-M. Choi, A. Schleife, and D. G. Cahill, Optical-helicity-driven magnetization dynamics in metallic ferromagnets, *Nature Communications* **8**, 15085 (2017).
- [48] R. John, M. Berritta, D. Hinzke, C. Müller, T. Santos, H. Ulrichs, P. Nieves, J. Walowski, R. Mondal, O. Chubykalo-Fesenko, J. McCord, P. M. Oppeneer, U. Nowak, and M. Münzenberg, Magnetisation switching of FePt nanoparticle recording medium by femtosecond laser pulses, *Scientific Reports* **7**, 4114 (2017).
- [49] A. V. Kimel, A. Kirilyuk, P. A. Usachev, R. V. Pisarev, A. M. Balbashov, and T. Rasing, Ultrafast non-thermal control of magnetization by instantaneous photomagnetic pulses, *Nature* **435**, 655 (2005).
- [50] A. V. Kimel and M. Li, Writing magnetic memory with ultrashort light pulses, *Nature Reviews Materials* **4**, 189 (2019).
- [51] S. Wust, C. Seibel, H. Meer, P. Herrgen, C. Schmitt, L. Baldradi, R. Ramos, T. Kikkawa, E. Saitoh, O. Gomonay, J. Sinova, Y. Mokrousov, H. C. Schneider, M. Kläui, B. Rethfeld, B. Stadtmüller, and M. Aeschlimann, Indirect optical manipulation of the antiferromagnetic order of insulating NiO by ultrafast interfacial energy transfer (2022), [arXiv:2205.02686 \[cond-mat.mtrl-sci\]](https://arxiv.org/abs/2205.02686).
- [52] D. Wortmann, G. Michalicek, N. Baadji, M. Betzinger, G. Bihlmayer, J. Bröder, T. Burnus, J. Enkovaara, F. Freimuth, C. Friedrich, C.-R. Gerhorst, S. Granberg Cauchi, U. Grytsiuk, A. Hanke, J.-P. Hanke, M. Heide, S. Heinze, R. Hilgers, H. Janssen, D. A. Klüppelberg, R. Kovacik, P. Kurz, M. Lezaic, G. K. H. Madsen, Y. Mokrousov, A. Neukirchen, M. Redies, S. Rost, M. Schlipf, A. Schindlmayr, M. Winkelmann, and S. Blügel, *Fleur* (2023).
- [53] J. P. Perdew, K. Burke, and M. Ernzerhof, Generalized Gradient Approximation Made Simple, *Phys. Rev. Lett.* **77**, 3865 (1996).
- [54] C. Li, A. J. Freeman, H. J. F. Jansen, and C. L. Fu, Magnetic anisotropy in low-dimensional ferromagnetic systems: Fe monolayers on Ag(001), Au(001), and Pd(001) substrates, *Phys. Rev. B* **42**, 5433 (1990).
- [55] A. Jain, S. P. Ong, G. Hautier, W. Chen, W. D. Richards, S. Dacek, S. Cholia, D. Gunter, D. Skinner, G. Ceder, and K. A. Persson, Commentary: The Materials Project: A materials genome approach to accelerating materials innovation, *APL Materials* **1**, 011002 (2013), <https://pubs.aip.org/aip/apm/article-pdf/doi/10.1063/1.4812323/13163869/011002.1.online.pdf>.
- [56] D. Singh, Ground-state properties of lanthanum: Treatment of extended-core states, *Phys. Rev. B* **43**, 6388 (1991).
- [57] G. Pizzi, V. Vitale, R. Arita, S. Blügel, F. Freimuth, G. Géranton, M. Gibertini, D. Gresch, C. Johnson, T. Koretsune, J. Ibañez-Azpiroz, H. Lee, J.-M. Lihm, D. Marchand, A. Marrazzo, Y. Mokrousov, J. I. Mustafa, Y. Nohara, Y. Nomura, L. Paulatto, S. Poncé, T. Ponweiser, J. Qiao, F. Thöle, S. S. Tsirkin, M. Wierzbowska, N. Marzari, D. Vanderbilt, I. Souza, A. A. Mostofi, and J. R. Yates, Wannier90 as a com-

munity code: new features and applications, [Journal of Physics:](#)

[Condensed Matter](#) **32**, 165902 (2020).